Detecting the superfluid critical momentum of Bose gases in optical lattices through dipole oscillations

Takuya Saito,[1,*] Ippei Danshita,[2,†] Takeshi Ozaki,[1] and Tetsuro Nikuni[1]

[1]*Department of Physics, Faculty of Science, Tokyo University of Science, 1-3 Kagurazaka, Shinjuku, Tokyo 162-8601, Japan*

[2]*Computational Condensed Matter Physics Laboratory, RIKEN, 2-1 Hirosawa, Wako, Saitama 351-0198, Japan*

(Received 28 March 2012; published 21 August 2012)

We study the stability of superflow of Bose gases in optical lattices by analyzing the Bose-Hubbard model within the Gutzwiller mean-field approximation. We calculate the excitation spectra of the homogeneous Bose-Hubbard model at unit filling to determine the critical momenta for the Landau and dynamical instabilities. These two critical momenta are shown to approach each other when the on-site interaction increases towards the Mott transition point. In order to make a direct connection with realistic experiments, we next take into account a parabolic trapping potential and compute the real-time dynamics of dipole oscillations induced by suddenly displacing the trap center. We consider the following two cases: standard soft-core bosons, whose interparticle interactions include the on-site one only; and hard-core bosons with long-range dipole-dipole interactions. For both cases, we show that the dipole oscillation is significantly damped when the maximum local momentum exceeds a certain threshold, which quantitatively agrees with the critical momentum for the dynamical instability in the homogeneous system. In the case of dipolar hard-core bosons, the dynamical instability of dipole oscillations leads to the formation of checkerboard density waves in the superfluid phase near the boundary to the supersolid phase.

DOI: 10.1103/PhysRevA.86.023623 PACS number(s): 03.75.Lm, 67.85.De, 67.85.Hj, 05.60.Gg

I. INTRODUCTION

Since the observation of the quantum phase transition from superfluid (SF) to Mott insulator (MI) [1], systems of ultracold gases confined in optical lattices have provided an ideal venue for studying strong correlation physics [2]. Many interesting properties of strongly correlated ultracold gases have been revealed in recent experiments, including excitation spectra [3–6], quantum criticality [7], and particle transport [8–10].

In particular, transport properties have attracted much interest, in connection with the SF critical momentum above which superflow breaks down. In experiments with ultracold gases in optical lattices, transport is investigated by using a moving optical lattice [9,11,12] or suddenly displacing the parabolic trapping potential to induce a dipole oscillation [8,10,13]. In the weakly interacting regime, where the Gross-Pitaevskii (GP) mean-field approximation is valid, it has been shown that the critical momentum in a trapped system at low temperatures agrees quantitatively with that for the dynamical instability (DI) in the homogeneous lattice system [11–15], regardless of whether one uses the trap displacement or the moving optical lattice. In the intermediate and strongly interacting regimes, while the agreement in the critical momenta of the trapped and untrapped systems has been obtained when the moving optical lattice is used [9,16,17], it remains unclear whether this is also the case for the trap displacement.

In addition to optical lattices, new possibilities for the study of strong correlation physics have been opened up by the creation of ultracold atomic gases with strong magnetic dipole-dipole interactions [18,19] and gases of polar molecules [20,21]. It has been predicted that when a dipolar Bose gas is loaded on an optical lattice, there exist supersolid (SS) phases that possess both diagonal (crystalline) and off-diagonal (SF) long-range order [22–29]. Danshita and Yamamoto have studied the critical momenta of dipolar Bose gases in a two-dimensional (2D) optical lattices and suggested that some properties of the critical momenta can be used to identify SS phases [28]. More specifically, the critical momenta of the SS phases are finite, in contrast to the insulating phases, such as MI and density wave phases, and significantly smaller than that for the SF phase. Since the analyses in Ref. [28] have been done in a homogeneous lattice system, it is important to investigate the critical momenta of dipolar Bose gases in the presence of a parabolic trap in order to make the suggestion more convincing.

In this paper, using the Gutzwiller approximation, we study SF transport of Bose gases in optical lattices with and without the dipole-dipole interactions. First, we analyze the critical momenta of Bose gases without the dipole-dipole interactions at unit filling in homogeneous 1D, 2D, and 3D optical lattices by calculating the excitation spectra. We locate the boundaries to the Landau instability (LI) and the DI. Second, solving the equation of motion numerically, we simulate the dynamics of dipole oscillations of Bose gases confined in a parabolic potential in both the absence and the presence of the dipole-dipole interactions. For both cases, we find significant damping of the dipole oscillations when the maximum local momentum exceeds a certain critical value, and the critical value coincides with the critical momentum for the DI in homogeneous lattice systems. We also find a parameter region in which the dipole-oscillation mode is resonantly coupled with the breathing mode. When dipole-dipole interactions are present and the system is in the SF state close to the SS phase, we show that the DI of a dipole oscillation is followed by the formation of checkerboard density waves, as predicted in Ref. [28].

*takuya.saito.880217@gmail.com
†danshita@riken.jp

This paper is organized as follows. In Sec. II, we introduce the Bose-Hubbard Hamiltonian and our formulation of the problem based on the Gutzwiller mean-field approximation. In Sec. III, we calculate the critical momenta at unit filling in homogeneous 1D, 2D, and 3D optical lattices from the excitation spectra. In Sec. IV, we calculate the dipole oscillations to determine the critical momenta in the presence of a parabolic trapping potential. In Sec. V, we analyze the dipole oscillations of dipolar hardcore bosons. In Sec. VI, we summarize our results.

II. MODEL AND FORMULATION

A. Bose-Hubbard model

We consider a system of ultracold Bose gases confined in deep optical lattices combined with a parabolic trap. This system is well described by the Bose-Hubbard model [30,31],

$$\hat{H} = -J\sum_{\mathbf{j}}\sum_{\alpha=1}^{d}(\hat{a}_{\mathbf{j}}^{\dagger}\hat{a}_{\mathbf{j}+\mathbf{e}_\alpha} + \text{H.c.}) + \frac{U}{2}\sum_{\mathbf{j}}\hat{n}_{\mathbf{j}}(\hat{n}_{\mathbf{j}}-1) + \sum_{\mathbf{j}}(\epsilon_{\mathbf{j}}-\mu)\hat{n}_{\mathbf{j}}, \tag{1}$$

where $\epsilon_{\mathbf{j}} = \Omega|a\mathbf{j} - \mathbf{r}_0(t)|^2$. a and d represent the lattice constant and the spatial dimension. The vectors $\mathbf{j}$ and $\mathbf{e}_\alpha$ denote the site index and a unit vector in direction α, where the directions $\alpha = 1$, 2, and 3 mean the x, y, and z directions. $\hat{a}_{\mathbf{j}}$ ($\hat{a}_{\mathbf{j}}^{\dagger}$) is the annihilation (creation) operator and $\hat{n}_{\mathbf{j}} = \hat{a}_{\mathbf{j}}^{\dagger}\hat{a}_{\mathbf{j}}$ is the number operator at site $\mathbf{j}$. J, U, Ω, and μ are the hopping amplitude, the on-site interaction parameter, the curvature of the parabolic trap, and the chemical potential, respectively. We fix the trap curvature to be $\Omega/J = 0.01$ when we consider dipole oscillations of Bose gases in optical lattices in the presence of a parabolic trap. We assume that dipole oscillations are induced by displacing the trap center in the x direction as $\boldsymbol{r}_0(t) = Da\theta(t)\hat{\boldsymbol{e}}_1$, where $\theta(t)$ is the step function. We control the momentum of Bose gases by changing the displacement Da. Henceforth, we adopt the units in which $J = \hbar = a = 1$ except in the figures and their captions.

B. Gutzwiller approximation

In order to calculate the ground states, the excitation spectra, and the real-time dynamics of Bose gases in optical lattices, we use the Gutzwiller approximation, in which the many-body wave function is assumed to be a single product of local states as [32]

$$|\Psi_G\rangle = \prod_{\mathbf{j}}\sum_{n} f_{\mathbf{j},n}(t)|n\rangle_{\mathbf{j}}, \tag{2}$$

where $|n\rangle_{\mathbf{j}}$ represents the local Fock state at the site $\mathbf{j}$ and the normalization condition for coefficient $f_{\mathbf{j},n}$ is $\sum_n |f_{\mathbf{j},n}|^2 = 1$. Minimizing the effective action, $\int dt\langle\Psi_G|i\frac{d}{dt} - \hat{H}|\Psi_G\rangle$, with respect to $f_{\mathbf{j},n}^*$, one can derive the equation of motion for $f_{\mathbf{j},n}$,

$$i\frac{df_{\mathbf{j},n}(t)}{dt} = -\sum_{\alpha=1}^{d}\left[\sqrt{n}\,f_{\mathbf{j},n-1}\left(\Phi_{\mathbf{j}-\mathbf{e}_\alpha} + \Phi_{\mathbf{j}+\mathbf{e}_\alpha}\right) + \sqrt{n+1}\,f_{\mathbf{j},n+1}\left(\Phi_{\mathbf{j}-\mathbf{e}_\alpha}^* + \Phi_{\mathbf{j}+\mathbf{e}_\alpha}^*\right)\right] + \left[\frac{U}{2}n(n-1) + (\epsilon_{\mathbf{j}}-\mu)n\right]f_{\mathbf{j},n}, \tag{3}$$

where $\Phi_j \equiv \langle\Psi_G|\hat{a}_j|\Psi_G\rangle = \sum_n \sqrt{n}\,f_{\mathbf{j},n-1}^* f_{\mathbf{j},n}$ is the SF order parameter. While Eq. (3) obviously describes the real-time dynamics, it also allows us to calculate the ground states by solving it in imaginary time [33]. A steady solution takes the form of $f_{\mathbf{j},n}(t) = \tilde{f}_{\mathbf{j},n}e^{-i\tilde{\omega}_{\mathbf{j}}t}$, where $\tilde{f}_{\mathbf{j},n}$ is time independent and the phase factor $\tilde{\omega}_{\mathbf{j}}$ is given by

$$\tilde{\omega}_{\mathbf{j}} = -\sum_{\alpha=1}^{d}\left[\left(\tilde{\Phi}_{\mathbf{j}-\mathbf{e}_\alpha} + \tilde{\Phi}_{\mathbf{j}+\mathbf{e}_\alpha}\right)\tilde{\Phi}_{\mathbf{j}}^* + \left(\tilde{\Phi}_{\mathbf{j}-\mathbf{e}_\alpha}^* + \tilde{\Phi}_{\mathbf{j}+\mathbf{e}_\alpha}^*\right)\tilde{\Phi}_{\mathbf{j}}\right] + \sum_n\left[\frac{U}{2}(n-1) - \mu_{\mathbf{j}}\right]n|\tilde{f}_{\mathbf{j},n}|^2. \tag{4}$$

Here, $\mu_{\mathbf{j}} = \mu - \epsilon_{\mathbf{j}}$ is the effective chemical potential at site $\mathbf{j}$ and $\tilde{\Phi}_{\mathbf{j}} = \sum_n \sqrt{n}\,\tilde{f}_{\mathbf{j},n-1}^*\tilde{f}_{\mathbf{j},n}$ is the SF order parameter for the steady state. We explain how to calculate the excitation spectra from Eq. (3) in the next subsection.

The Gutzwiller approximation has often been applied to the Bose-Hubbard model in order to analyze various phenomena and properties of Bose gases in optical lattices. This approximation is more accurate in higher dimensions because of its mean-field nature. Indeed, thorough comparisons with experiments have shown that it can quantitatively describe several interesting properties in three dimensions, such as the excitation spectra [6] and critical momenta [9]. The qualitative validity of this approximation is thought to hold also in two dimensions, given that it correctly captures the order of the SF-to-MI quantum phase transition. In contrast, it is widely known that the Gutzwiller approximation fails miserably in one dimension except for very weak interactions $U \ll 1$. Regarding the SF-to-MI transition, for instance, the transition in one dimension is of the Berezinskii-Kosterlitz-Thouless type and the critical value of U/J at unit filling is $(U/J)_c \simeq 3.4$ according to accurate DMRG calculations [34]. However, the Gutzwiller approximation predicts the second-order transition and $(U/J)_c = 11.7$. Nevertheless, in the present paper we analyze 1D systems using the Gutzwiller approximation because the simplicity of 1D systems is very useful to illustrate basic properties of transport that hold in the level of the approximation. Note that in Refs. [16,17] the Gutzwiller approximation has been used for calculating the critical momentum in one dimension in a similar spirit.

C. Excitation spectrum

Previous works have described prescriptions for calculating the excitation spectra of the homogeneous Bose-Hubbard model within the Gutzwiller approximation [23,35], and the prescriptions have been used to study several interesting properties, such as the excitations of soft-core dipolar

bosons [36] and the stability of dark solitons [37]. We analyze the excitation spectra not only to investigate the stability of Bose gases in homogeneous systems, but also to obtain collective-mode frequencies in trapped systems. While Kovrizhin *et al*. have used an extended version of the prescriptions to calculate the excitations in trapped systems [38], they have not explicitly explained their formulations. In this subsection, we present a detailed explanation of the extended version that allows us to deal with spatially inhomogeneous systems.

We consider a small fluctuation $\delta f_{\mathbf{j},n}$ around a steady solution $\tilde{f}_{\mathbf{j},n}$,

$$f_{\mathbf{j},n}(t) = [\tilde{f}_{\mathbf{j},n} + \delta f_{\mathbf{j},n}(t)]e^{-i\tilde{\omega}_{\mathbf{j}}t}. \tag{5}$$

We substitute Eq. (5) into Eq. (3) and linearize the equation of motion with respect to the fluctuation $\delta f_{\mathbf{j},n}$. The Bogoliubov transformation on the fluctuation,

$$\delta f_{\mathbf{j},n} = u_{\mathbf{j},n}e^{-i\omega t} + v^*_{\mathbf{j},n}e^{i\omega^* t}, \tag{6}$$

leads to the following linear equations:

$$\begin{aligned}
\omega u_{\mathbf{j},n} = &-\sum_m\sum_{\alpha=1}^{d}\Big[\Big\{\sqrt{nm}\,\tilde{f}_{\mathbf{j},n-1}\tilde{f}^*_{\mathbf{j}-\mathbf{e}_\alpha,m-1} + \sqrt{(n+1)(m+1)}\,\tilde{f}_{\mathbf{j},n+1}\tilde{f}^*_{\mathbf{j}-\mathbf{e}_\alpha,m+1}\Big\}u_{\mathbf{j}-\mathbf{e}_\alpha,m} + \Big\{\sqrt{nm}\,\tilde{f}_{\mathbf{j},n-1}\tilde{f}^*_{\mathbf{j}+\mathbf{e}_\alpha,m-1}\\
&+\sqrt{(n+1)(m+1)}\,\tilde{f}_{\mathbf{j},n+1}\tilde{f}^*_{\mathbf{j}+\mathbf{e}_\alpha,m+1}\Big\}u_{\mathbf{j}+\mathbf{e}_\alpha,m} + \Big\{\sqrt{n(m+1)}\,\tilde{f}_{\mathbf{j},n-1}\tilde{f}_{\mathbf{j}-\mathbf{e}_\alpha,m+1} + \sqrt{(n+1)m}\,\tilde{f}_{\mathbf{j},n+1}\tilde{f}_{\mathbf{j}-\mathbf{e}_\alpha,m-1}\Big\}v_{\mathbf{j}-\mathbf{e}_\alpha,m}\\
&+\Big\{\sqrt{n(m+1)}\,\tilde{f}_{\mathbf{j},n-1}\tilde{f}_{\mathbf{j}+\mathbf{e}_\alpha,m+1} + \sqrt{(n+1)m}\,\tilde{f}_{\mathbf{j},n+1}\tilde{f}_{\mathbf{j}+\mathbf{e}_\alpha,m-1}\Big\}v_{\mathbf{j}+\mathbf{e}_\alpha,m}\Big] - \sum_{\alpha=1}^{d}\Big[\sqrt{n}\big(\tilde{\Phi}_{\mathbf{j}-\mathbf{e}_\alpha} + \tilde{\Phi}_{\mathbf{j}+\mathbf{e}_\alpha}\big)u_{\mathbf{j},n-1}\\
&+\sqrt{n+1}\big(\tilde{\Phi}^*_{\mathbf{j}-\mathbf{e}_\alpha} + \tilde{\Phi}^*_{\mathbf{j}+\mathbf{e}_\alpha}\big)u_{\mathbf{j},n+1}\Big] + \left[\frac{U}{2}n(n-1) - n\mu_{\mathbf{j}} - \tilde{\omega}_{\mathbf{j}}\right]u_{\mathbf{j},n},
\end{aligned} \tag{7}$$

$$\begin{aligned}
-\omega v_{\mathbf{j},n} = &-\sum_m\sum_{\alpha=1}^{d}\Big[\Big\{\sqrt{nm}\,\tilde{f}^*_{\mathbf{j},n-1}\tilde{f}_{\mathbf{j}-\mathbf{e}_\alpha,m-1} + \sqrt{(n+1)(m+1)}\,\tilde{f}^*_{\mathbf{j},n+1}\tilde{f}_{\mathbf{j}-\mathbf{e}_\alpha,m+1}\Big\}v_{\mathbf{j}-\mathbf{e}_\alpha,m} + \Big\{\sqrt{nm}\,\tilde{f}^*_{\mathbf{j},n-1}\tilde{f}_{\mathbf{j}+\mathbf{e}_\alpha,m-1}\\
&+\sqrt{(n+1)(m+1)}\,\tilde{f}^*_{\mathbf{j},n+1}\tilde{f}_{\mathbf{j}+\mathbf{e}_\alpha,m+1}\Big\}v_{\mathbf{j}+\mathbf{e}_\alpha,m} + \Big\{\sqrt{n(m+1)}\,\tilde{f}^*_{\mathbf{j},n-1}\tilde{f}^*_{\mathbf{j}-\mathbf{e}_\alpha,m+1} + \sqrt{(n+1)m}\,\tilde{f}^*_{\mathbf{j},n+1}\tilde{f}^*_{\mathbf{j}-\mathbf{e}_\alpha,m-1}\Big\}u_{\mathbf{j}-\mathbf{e}_\alpha,m}\\
&+\Big\{\sqrt{n(m+1)}\,\tilde{f}^*_{\mathbf{j},n-1}\tilde{f}^*_{\mathbf{j}+\mathbf{e}_\alpha,m+1} + \sqrt{(n+1)m}\,\tilde{f}^*_{\mathbf{j},n+1}\tilde{f}^*_{\mathbf{j}+\mathbf{e}_\alpha,m-1}\Big\}u_{\mathbf{j}+\mathbf{e}_\alpha,m}\Big] - \sum_{\alpha=1}^{d}\Big[\sqrt{n}\big(\tilde{\Phi}^*_{\mathbf{j}-\mathbf{e}_\alpha} + \tilde{\Phi}^*_{\mathbf{j}+\mathbf{e}_\alpha}\big)v_{\mathbf{j},n-1}\\
&+\sqrt{n+1}\big(\tilde{\Phi}_{\mathbf{j}-\mathbf{e}_\alpha} + \tilde{\Phi}_{\mathbf{j}+\mathbf{e}_\alpha}\big)v_{\mathbf{j},n+1}\Big] + \left[\frac{U}{2}n(n-1) - n\mu_{\mathbf{j}} - \tilde{\omega}_{\mathbf{j}}\right]v_{\mathbf{j},n}.
\end{aligned} \tag{8}$$

Solving these equations, one obtains the frequencies ω and the wave functions $(u_{\mathbf{j},n}, v_{\mathbf{j},n})$ of excitations, which allow us to discriminate the stability of a steady state [39]. When all the excitations satisfy the condition $\mathcal{N}\omega \geqslant 0$, the steady state is stable, where $\mathcal{N} = \sum_{\mathbf{j}}\sum_n(|u_{\mathbf{j},n}|^2 - |v_{\mathbf{j},n}|^2)$ is the normalization constant and $\mathcal{N}\omega$ describes the energy change associated with low-amplitude oscillations given by Eq. (6). If there exist excitations satisfying $\mathcal{N}\omega < 0$, the state is energetically unstable. This instability is called the LI. The emergence of excitations with complex frequencies, i.e., $|\mathrm{Im}[\omega]| > 0$, signals the DI, which means exponential growth of the fluctuation in time. In a system of atomic gases at sufficiently low temperatures, while the LI cannot destabilize the system because of the lack of energy-dissipation processes, the DI can drastically break down the system [12,40,41]. Hence, it is important to calculate the critical momentum for the DI, even though it is always larger than the Landau critical momentum [39].

We show in Sec. IV that significant damping of dipole oscillations occurs when the maximum local momentum in a trapped system exceeds the critical momentum for the DI in a homogeneous system.

III. CRITICAL MOMENTA IN HOMOGENEOUS OPTICAL LATTICES

In this section, we numerically solve Eqs. (7) and (8) to obtain the excitation spectra for homogeneous Bose-Hubbard systems at $\nu = 1$ in one, two, and three dimensions, where ν is the filling factor. Using the discriminant described in the previous section, we determine the critical momenta for the LI and the DI. Note that the critical momenta for the DI have been obtained in Refs. [16,17] by solving the equation of motion, (3), in real time in a situation where the on-site interaction U or the flow momentum is slowly increased. A clear advantage of our method over the previous work is that the critical momenta for the LI is also available. We also emphasize that one can calculate the critical momenta for the DI more accurately. In the limit of $U \to 0$, for instance, while the critical momentum obtained in Refs. [16,17] is a little larger than the prediction by the GP mean-field theory, i.e., $p = \pi/2$ [42], our method gives a precise agreement with the GP prediction as we see below.

To calculate the excitation spectra for moving Bose gases, we introduce the phase twist term in Eq. (1) as

$$\hat{a}^\dagger_{\mathbf{j}}\hat{a}_{\mathbf{j}+\mathbf{e}_\alpha} \to \hat{a}^\dagger_{\mathbf{j}}\hat{a}_{\mathbf{j}+\mathbf{e}_\alpha}e^{i\mathbf{p}\cdot\mathbf{e}_\alpha}, \tag{9}$$

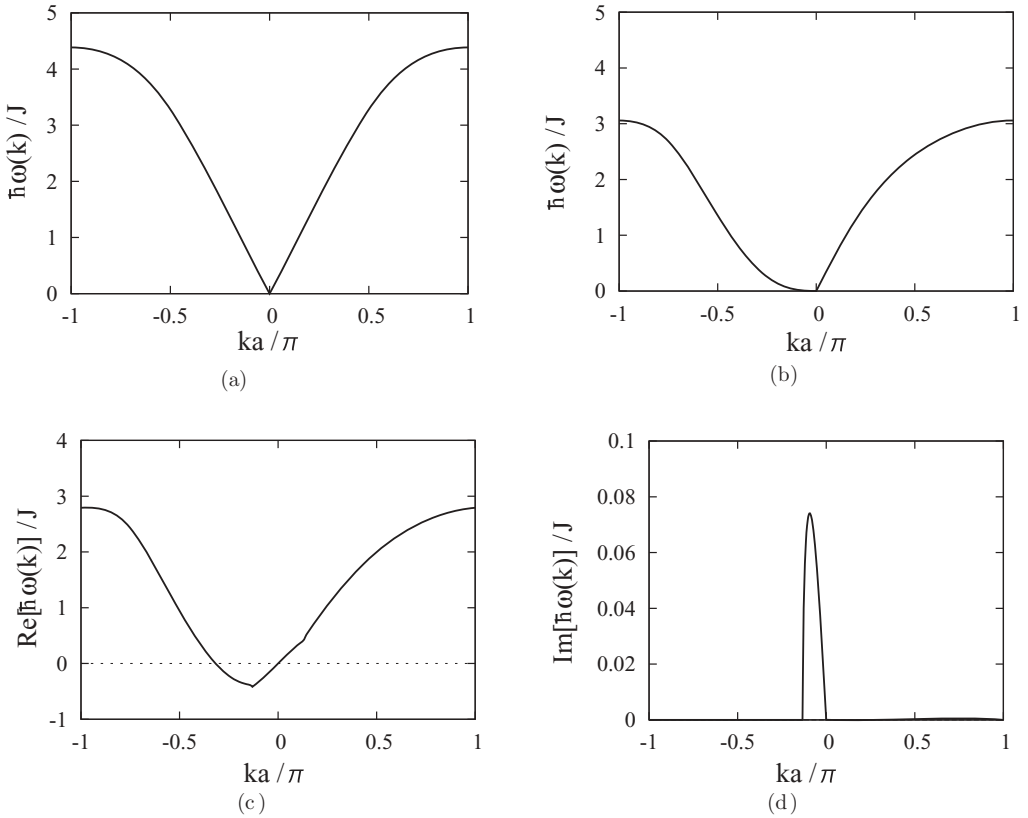

FIG. 1. Excitation spectra $\hbar\omega(k)/J$ in 1D homogeneous optical lattices for $U/J = 3$, $\nu = 1$, and different values of $pa/\hbar$. (a) $pa/\hbar = 0$; (b) $pa/\hbar = p_{\rm LI}a/\hbar \simeq 0.85$, where the LI sets in; (c, d) $pa/\hbar = 0.94 > p_{\rm DI1}a/\hbar$.

which represents the situation where the optical lattice is moving at a constant momentum $-\mathbf{p}$. Forcing the coefficients $f_{\mathbf{j},n}$ to be real numbers, we carry out imaginary-time evolution of Eq. (3) to obtain the steady state with zero momentum, which is equivalent to a state with momentum $\mathbf{p}$ in a static optical lattice. Substituting the coefficients $\tilde{f}_{\mathbf{j},n}$ of the steady state into Eqs. (7) and (8) and solving them, we obtain the excitation spectra of the current-carrying state.

In Fig. 1, we show the excitation spectra of Bose gases in 1D homogeneous optical lattices for $U = 3$ and different values of the flow momentum p. We plot the first branch of the excitations, which corresponds to the well-known Bogoliubov spectrum, because only this branch is relevant to the LI and the DI in most of the parameter regions. When $pa/\hbar = 0$, this branch has a phonon dispersion at $|k| \ll 1$ [Fig. 1(a)]. When p increases, the slope of the phonon dispersion for $k < 0$ decreases, and it reaches 0 at $p = p_{\rm LI} \simeq 0.85$ as shown in Fig. 1(b). This signals the onset of the LI. When p increases further and exceeds a certain threshold, the excitations at $|k| \ll 1$ have a finite imaginary part, which signals the DI. We call this threshold $p_{\rm DI1}$.

In Fig. 2, we show the critical momenta for the LI [dashed (red) lines] and the DI caused by excitations with $|k| \ll 1$ [solid (black) lines] in one, two, and three dimensions. In any dimensions, $p_{\rm LI} \to 0$ and $p_{\rm DI1} \to \pi/2$ when $U \to 0$. When U increases, $p_{\rm DI1}$ decreases monotonically and $p_{\rm LI}$ approaches

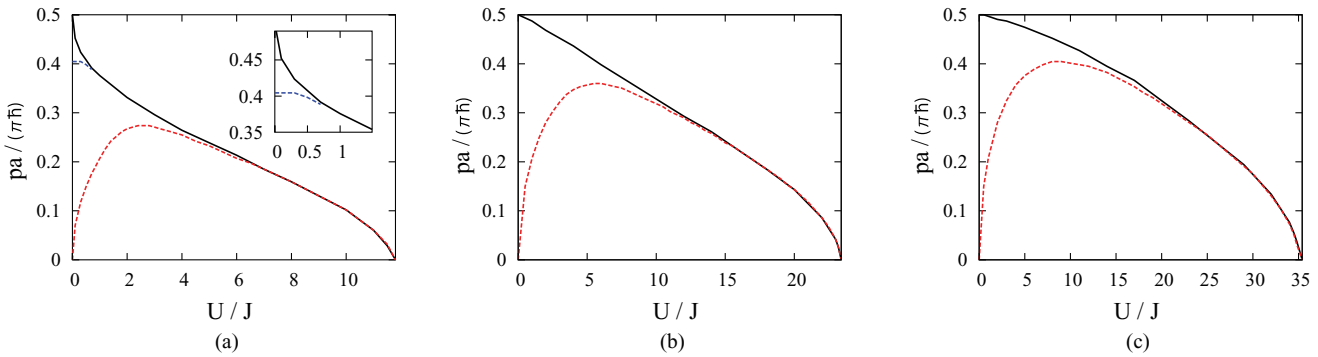

FIG. 2. (Color online) Critical momenta versus U/J in homogeneous optical lattices for $\nu = 1$: (a) 1D, (b) 2D, and (c) 3D. Dashed (red), solid (black), and dotted (blue) lines represent the critical momenta for the LI ($p_{\rm LI}a/\hbar$), the DI caused by excitations with long wavelengths ($p_{\rm DI1}a/\hbar$), and the DI caused by excitations with short wavelengths ($p_{\rm DI2}a/\hbar$).

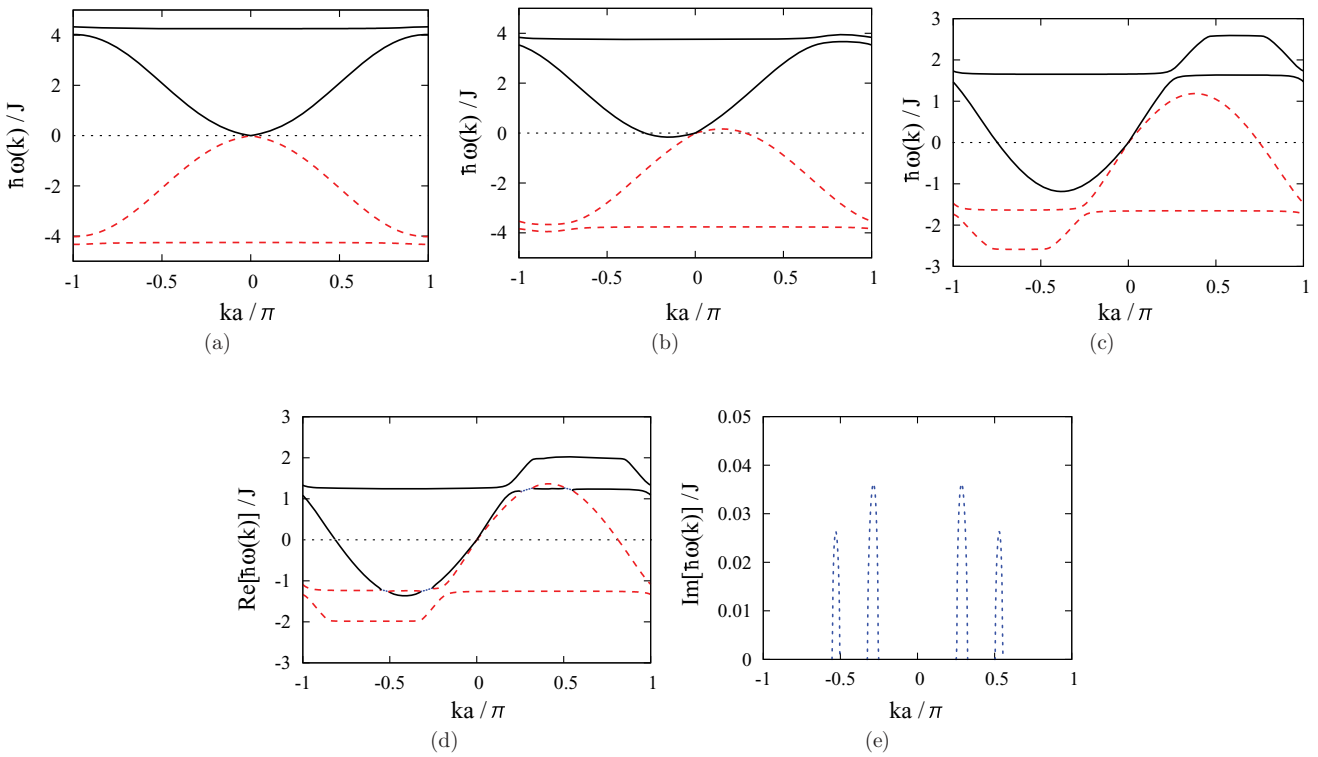

FIG. 3. (Color online) Excitation spectra $\hbar\omega(k)/J$ in 1D homogeneous optical lattices for the weak interaction $U/J = 0.1$, $\nu = 1$, and different values of $pa/\hbar$; (a) $pa/\hbar = 0$; (b) $pa/\hbar = 0.5$, where the avoided crossing of the first and second branches starts to occur; (c) $pa/\hbar = 1.2$; (d, e) $pa/\hbar = 1.3$, where excitations with short wavelengths cause the DI. Solid (black), dashed (red), and dotted (blue) lines represent the normal modes, the antimodes, and the modes whose imaginary part is finite.

p_{DI1}. In the strongly interacting region ($U \gtrsim U_c/2$), p_{LI} takes almost the same value as p_{DI1}, and both momenta reach 0 at $U = U_c$, where U_c denotes the SF-MI transition point. The behaviors of p_{DI1} are consistent with the work in Refs. [16,17].

When the interaction is sufficiently weak in one dimension, a DI caused by excitations with short wavelengths precedes the DI caused by excitations with $|k| \ll 1$. The critical momentum for this DI p_{DI2} is plotted by the dotted (blue) line in Fig. 2(a). To understand this instability, we show in Fig. 3 the excitation spectra including the first branch (Bogoliubov mode), the second branch, and the antimodes of the two branches [43] for $U = 0.1$ and different values of p. Note that the second branch becomes the amplitude mode in the strongly interacting region. When p increases, the second branch declines and exhibits an avoided crossing with the first branch as shown in Figs. 3(b) and 3(c). With further increases in p, the second (first) branch is coupled with the antimode of the first (second) branch and these coupled modes cause the DI [39]. We suggest that this DI leads to the formation of density waves with ordering vectors $k \simeq \pm 0.3\pi$ and $\pm 0.5\pi$. While this type of DI has been found previously in the presence of off-site interactions [28,44–46], this is the first example of such a DI in the standard Bose-Hubbard model only with the on-site interaction.

IV. DIPOLE OSCILLATIONS IN THE STANDARD BOSE-HUBBARD SYSTEM

In this section, we consider systems of Bose gases in 1D and 2D optical lattices combined with a parabolic trap. We fix the total number of particles to be $N = 45$ in 1D and $N = 3000$ in 2D lattices such that the Mott plateau at unit filling forms in the central region of the trap when U exceeds U_c. We first calculate the ground state via imaginary-time evolution of Eq. (3). We next calculate real-time dynamics subjected to a sudden displacement of the trap center that induces a dipole oscillation. Note that while similar dynamics have been studied in Refs. [38,47] using the same Gutzwiller approximation, the previous studies did not address the relation between dipole oscillations and critical momenta, which is our main interest here.

A. Stability and damping of dipole oscillations

To illustrate basic properties of the dynamics of dipole oscillations, we start our analyses with the 1D case. In Fig. 4, we show typical examples of the center-of-mass (c.m.) motion for stable and damped dipole oscillations. The amplitude of the dipole oscillation hardly changes as long as the displacement D is smaller than a certain critical value D_c as shown in Fig. 4(a). This dissipationless motion is a clear characteristic of superflow. In contrast, the oscillation is remarkably damped when D_c is exceeded [see Fig. 4(b)]. It is worth noting that the dynamics for these two cases can be clearly distinguished because the transition to the damped oscillation occurs very sharply. Thanks to this property, one can determine the critical displacement accurately.

It is shown in Fig. 4(b) that the oscillation is damped in a short time scale, within $t < 100\hbar/J$, and becomes almost undamped afterward. However, when D is sufficiently large compared to D_c, the breakdown of superflow is so significant

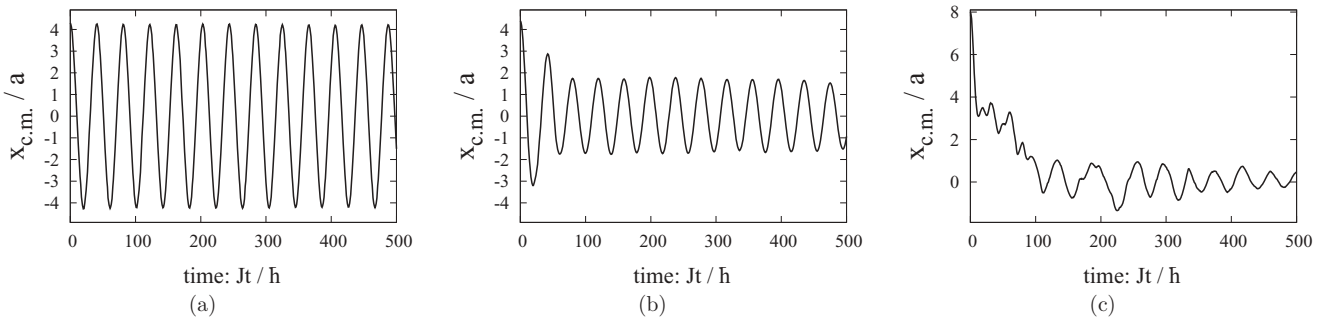

FIG. 4. Time evolution of the center-of-mass $x_{\mathrm{c.m.}}(t)/a$ in 1D optical lattices combined with the parabolic trap for $U/J = 6$. The maximum density of the initial state is 1.29. (a) Stable dipole oscillation at $D = 4.3$; (b) damped dipole oscillation at $D = 4.4$; (c) overdamped motion at $D = 8$.

that the c.m. motion is overdamped and never exhibits a stable oscillation as shown in Fig. 4(c), where $D = 8$.

B. Collective and local momentum

We characterize the transport in trapped systems by the collective momentum $\mathbf{p}_{\mathrm{col}}$ and local momentum $\mathbf{p}_{\mathbf{j}}$ and compare them with the critical momenta in homogeneous systems. Let us first define the collective momentum. The c.m. velocity is given by $\mathbf{v}_{\mathrm{c.m.}} = d\mathbf{x}_{\mathrm{c.m.}}/dt$, where $\mathbf{x}_{\mathrm{c.m.}} = \sum_{\mathbf{j}} \mathbf{j} n_{\mathbf{j}}/N$ denotes the c.m. position. Here $n_{\mathbf{j}} = \langle \Psi_G | \hat{n}_{\mathbf{j}} | \Psi_G \rangle = \sum_n n f^*_{\mathbf{j},n} f_{\mathbf{j},n}$ is the density at site $\mathbf{j}$. In the tight-binding regime, since the (quasi)momentum p^α in the α direction is related to the group velocity v^α as

$$v^\alpha = 2 \sin p^\alpha, \tag{10}$$

we define the collective momentum as

$$p^\alpha_{\mathrm{col}} = \sin^{-1}\left(\frac{v^\alpha_{\mathrm{c.m.}}}{2}\right). \tag{11}$$

Note that a different parameter to analyze the collective motion, i.e., $\mathbf{p}_{\mathrm{c.m.}} = \sum_{\mathrm{p}} \mathbf{p} n_{\mathbf{p}}/N$, was used in Refs. [16,17], where $n_{\mathbf{p}}$ is the momentum distribution. However, we adopt the quantity defined by Eq. (11) because it is more directly relevant to actual experiments in the sense that the c.m. velocity can be measured rather easily in the time-of-flight images as done in experiments in Refs. [8,10].

The local momentum $p^\alpha_{\mathbf{j}}$ means the momentum per particle of the local current $I^\alpha_{\mathbf{j}}$ flowing from site $\mathbf{j}$ to site $\mathbf{j} + \mathbf{e}_\alpha$, which is given by $I^\alpha_{\mathbf{j}} = (\Phi^*_{\mathbf{j}} \Phi_{\mathbf{j}+\mathbf{e}_\alpha} - \Phi_{\mathbf{j}} \Phi^*_{\mathbf{j}+\mathbf{e}_\alpha})/i$ within the Gutzwiller approximation. With this local current, the local velocity is expressed as

$$v^\alpha_{\mathbf{j}} = \frac{I^\alpha_{\mathbf{j}}}{\sqrt{n^{\mathrm{c}}_{\mathbf{j}} n^{\mathrm{c}}_{\mathbf{j}+\mathbf{e}_\alpha}}}, \tag{12}$$

where $n^{\mathrm{c}}_{\mathbf{j}} = |\Phi_{\mathbf{j}}|^2$ is the condensate density at site $\mathbf{j}$. From Eqs. (10) and (12), the local momentum is naturally defined as

$$p^\alpha_{\mathbf{j}} = \sin^{-1}\left(\frac{I^\alpha_{\mathbf{j}}}{2\sqrt{n^{\mathrm{c}}_{\mathbf{j}} n^{\mathrm{c}}_{\mathbf{j}+\mathbf{e}_\alpha}}}\right). \tag{13}$$

We show in the next section that significant damping of dipole oscillations occurs when the maximum local momentum in a trapped system exceeds the critical momentum for the DI in a homogeneous system.

In Fig. 5, we show snapshots of the local momentum p_j, the condensate density n^{c}_j, and the density n_j at the critical displacement $D = D_{\mathrm{c}}$ for a weak interaction, $U = 2$ [Fig. 5(a)], and a strong interaction, $U = 10$ [Fig. 5(b)]. The time is set such that the momentum of c.m. takes the maximum value during the time evolution. We define this time as t_{max}. For the weak interaction, the local momentum is almost constant. On the other hand, for the strong interaction in Fig. 5(b), the local momentum is significantly dependent on the position so that it peaks at unit-filling points. This happens because the condensate density in regions close to unit filling is strongly suppressed as a precursor of the formation of Mott plateaus. Due to the strong spatial dependence of the local momentum, the collective momentum is noticeably smaller than the maximum local momentum, especially near the Mott transition.

C. Critical momentum

In Fig. 6, we show the maximum local momentum p_{max} and the collective momentum p_{col} at $D = D_{\mathrm{c}}$ and $t = t_{\mathrm{max}}$ as functions of U. For comparison, we also plot the critical momenta p_{DI1} obtained in homogeneous systems at unit filling. We find that $p_{\mathrm{max}}(t = t_{\mathrm{max}})$ in the trapped system quantitatively agrees with p_{DI1}. In contrast, $p_{\mathrm{col}}(t = t_{\mathrm{max}})$ drastically deviates from p_{DI1}. These results lead to an important conclusion; to detect critical momenta for homogeneous lattice systems from dipole oscillations, one needs to measure the local momentum rather than the collective momentum, which can be measured relatively easily from the time-of-flight images [8,10,13]. While the local momentum has never been experimentally measured so far, it should be available in future experiments because recent experiments have developed techniques to address local observables at the scale of a single lattice site [7,48].

D. Mode coupling

We now focus on long-time dynamics of the dipole oscillation. In this case, we find that the dipole oscillation with damping and revival occurs below the critical momentum in a particular range at the interaction $U = 7.5$–7.8. Similar behaviors have been found in Refs. [38,47]. In Fig. 7, we

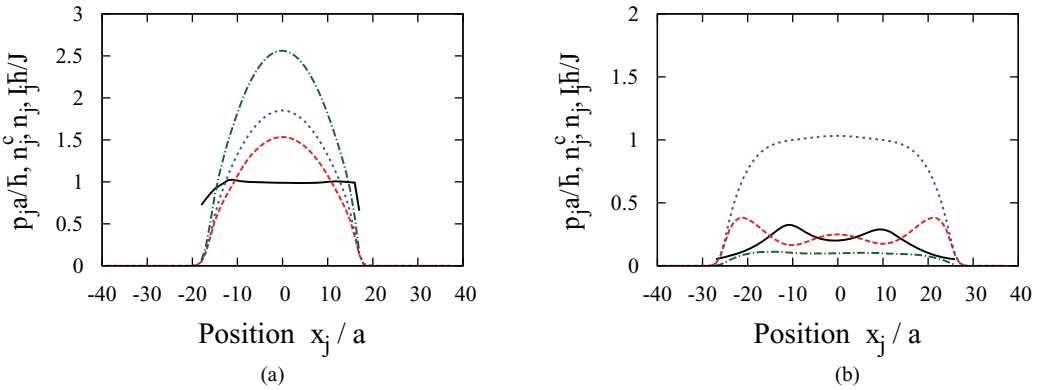

FIG. 5. (Color online) Local momentum $p_j a/\hbar$ [solid (black) line], local condensate density $n_j^c = |\Phi_j|^2$ [dashed (red) line], local density n_j [dotted (blue) line], local current $I_j\hbar/J$ [dot-dashed (green) line] in one dimension at $D = D_c$ and $t = t_{\max}$, where $U/J = 2$ (a) and $U/J = 10$ (b).

show this unusual oscillation for $U = 7.78$. To understand this phenomenon, we calculate the excitation spectrum by diagonalizing Eqs. (7) and (8). In Fig. 8(a), we plot the frequencies of the first and second modes, which correspond to the dipole mode and the breathing mode, respectively. We also show the ratio of the breathing-mode frequency ω_2 to the dipole-mode frequency ω_1 in Fig. 8(b). We find that the ratio ω_2/ω_1 is nearly equal to 2 in the regime where damping and revival occur. Therefore, this phenomenon can be interpreted as indicating that dipole and breathing modes are coupled by the nonlinear effect in Eq. (3). In this regime, although the amplitude of the dipole oscillation decreases due to this mode coupling even below the critical momentum, we can determine the critical momentum because the damping caused by mode coupling is much smaller than that caused by the DI.

V. DIPOLAR HARDCORE BOSONS

In this section, we consider dipolar bosons confined in 2D optical lattices combined with a parabolic trapping potential. For simplicity, we consider the hard-core limit ($U \to \infty$), in which the local Hilbert space is spanned only with $|0\rangle$ and $|1\rangle$, and we analyze this system using the Gutzwiller approximation as in the previous section. Thus, we treat exactly the same system (HCB) within the same formalism as in Ref. [28] except for the parabolic trap. To compare the critical momentum extracted from the dipole oscillations with that for the homogeneous lattice system at $\nu = 0.4$ in Ref. [28], we introduced the averaged density $\bar{n}_{\rm ctr} = (n_{\mathbf{0}} + n_{\mathbf{e}_1})/2$. We assume that the dipoles are polarized to the direction perpendicular to the lattice plane. This system is well described by the Bose-Hubbard model

$$\hat{H} = -J \sum_{\mathbf{j}} \sum_{\alpha=1}^{d} \left(\hat{a}_{\mathbf{j}}^{\dagger} \hat{a}_{\mathbf{j}+\mathbf{e}_\alpha} + \text{h.c.}\right) + \frac{V}{2} \sum_{\mathbf{j}\neq\mathbf{l}} \frac{\hat{n}_{\mathbf{j}}\hat{n}_{\mathbf{l}}}{r_{\mathbf{j},\mathbf{l}}^3} + \sum_{\mathbf{j}} (\epsilon_{\mathbf{j}} - \mu)\hat{n}_{\mathbf{j}}, \tag{14}$$

where V is the strength of dipole-dipole interaction, and $r_{\mathbf{j},\mathbf{l}} = a|\mathbf{j} - \mathbf{l}|$ is the distance between site $\mathbf{j}$ and site $\mathbf{l}$. Since the dipolar interaction potential decays as $\sim r_{\mathbf{j},\mathbf{l}}^{-3}$, we only include dipolar interactions in the range $r_{\mathbf{j},\mathbf{l}} \leqslant 7a$ to reduce the computational time. While the simulation time is proportional to the number of lattices M with a cutoff of the dipole interaction, it

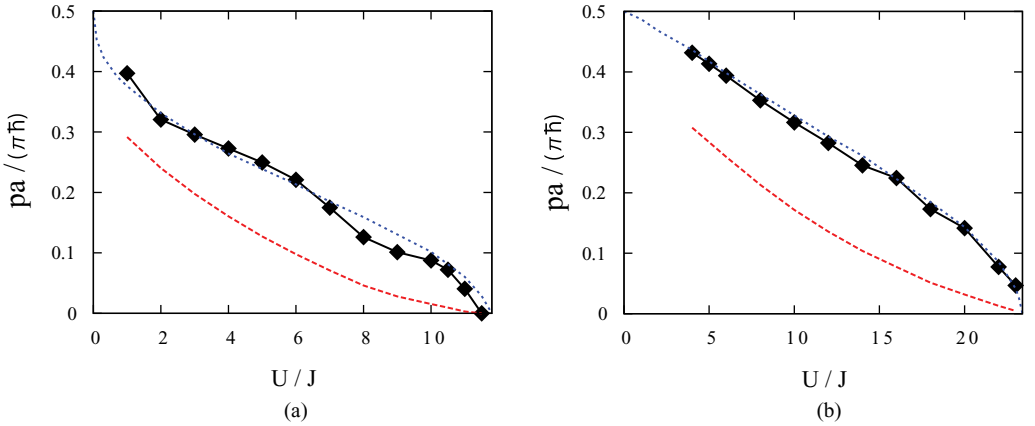

FIG. 6. (Color online) Maximum local momentum $p_{\max}a/(\pi\hbar)$ [solid (black) lines with symbols] and collective momentum $p_{\rm col}a/(\pi\hbar)$ [dashed (red) lines] at $D = D_c$ and $t = t_{\max}$ as functions of U/J: (a) 1D and (b) 2D. Dotted (blue) lines represent $p_{\rm DI}a/(\hbar\pi)$ in homogeneous lattice systems, which are plotted in Figs. 2(a) and 2(b) by solid (black) lines.

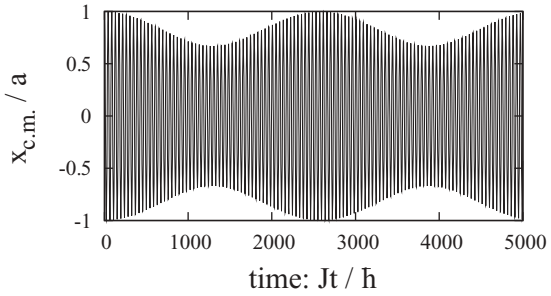

FIG. 7. Motion of the center-of-mass $x_{\mathrm{c.m.}}(t)/a$ with damping and revival in 1D optical lattices combined with a parabolic trap for $U/J = 7.78$.

is proportional to M^2 without a cutoff. Introducing this cutoff merely changes some quantitative characteristics of the system very slightly, and does not affect any qualitative properties, such as the quantum phase diagram and the critical momentum, when $V \lesssim 10$. We again adopt units of $\hbar = J = a = 1$.

A. Ground state

Let us calculate the ground state of Eq. (14). We fix the curvature of the parabolic potential and the total number of particles to be $\Omega = 0.01$ and $N = 900$. In this case, the ground state can be the following two types of states as long as $V < 4.5$. For small V, the dipolar gas in the ground state consists only of an SF region. When V is sufficiently large, the ground state has a region of the SS with a checkerboard density wave order around the trap center, and this SS region is surrounded by an SF region. As a metaphor, one may imagine a sunny-side-up egg whose yolk and white correspond to the SS and SF regions. In order to identify the transition between the two states, we show in Fig. 9 the average condensate density and the static structure factor around the center of the trap, which are defined as $n^{\mathrm{c}}_{\mathrm{ctr}} = \sum_{\mathbf{j}\in\mathrm{ctr}} |\Phi_{\mathbf{j}}|^2/25$ and $S_{\mathrm{ctr}}(\pi,\pi) = \sum_{\mathbf{j},\mathbf{l}\in\mathrm{ctr}} e^{i(\pi,\pi)\cdot(\mathbf{j}-\mathbf{l})}\langle n_j n_l\rangle/25$. Here $\sum_{\in\mathrm{ctr}}$ denotes the summation of the 5×5 sites around the center of the trap. By using these quantities, we identify the state with $n^{\mathrm{c}}_{\mathrm{ctr}} \neq 0$ and $S_{\mathrm{ctr}}(\pi,\pi) = 0$ as the SF state and the state with $n^{\mathrm{c}}_{\mathrm{ctr}} \neq 0$ and $S_{\mathrm{ctr}}(\pi,\pi) \neq 0$ as the SS state. We find that the boundary of the SF and the SS is $V = 3.26$. When $V > 4.5$, there emerge other SS and solid phases [26]. We do not analyze the region of $V > 4.5$, because our main focus is placed on the SF transport of the SF and checkerboard SS states.

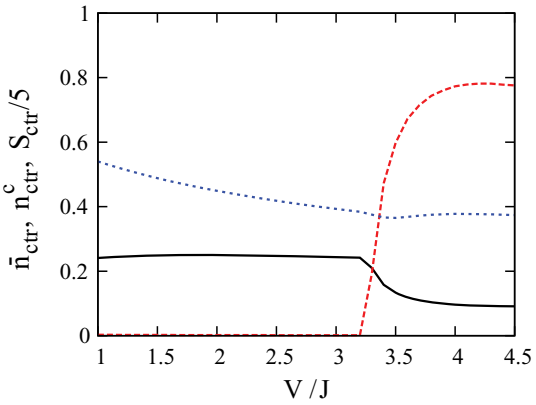

FIG. 9. (Color online) Average density $\bar{n}_{\mathrm{ctr}}$ [dotted (blue) line], average condensate density $n^{\mathrm{c}}_{\mathrm{ctr}}$ [solid (black) line], and static structure factor $S_{\mathrm{ctr}}(\pi,\pi)$ divided by 5 [dashed (red) line] around the trap center in the ground state of Eq. (14) are plotted as functions of V/J, where $\Omega/J = 0.01$ and $N = 900$.

To compare the critical momentum extracted from the dipole oscillations with that for the homogeneous lattice system at $\nu = 0.4$ in Ref. [28], we also plot the average density $\bar{n}_{\mathrm{ctr}} = (n_{\mathbf{0}} + n_{\mathbf{e}_i})/2$. For this purpose, we take the total number and the trap curvature such that the central average density is $\bar{n}_{\mathrm{ctr}} \simeq 0.4$ in the SS state as shown in Fig. 9. On the other hand, $\bar{n}_{\mathrm{ctr}}$ in the SF state ranges roughly between 0.4 and 0.6. However, this does not matter for the comparison because the critical momentum for the DI in the SF phase hardly depends on the density in the range of $0.4 < \nu < 0.6$.

B. Critical momentum

Having obtained the ground state of Eq. (14), we next calculate the dipole-oscillation dynamics following the method illustrated in the previous section. We find that the critical displacement D_{c} can be accurately determined also in the case of dipolar hard-core bosons. By the solid (black) line with

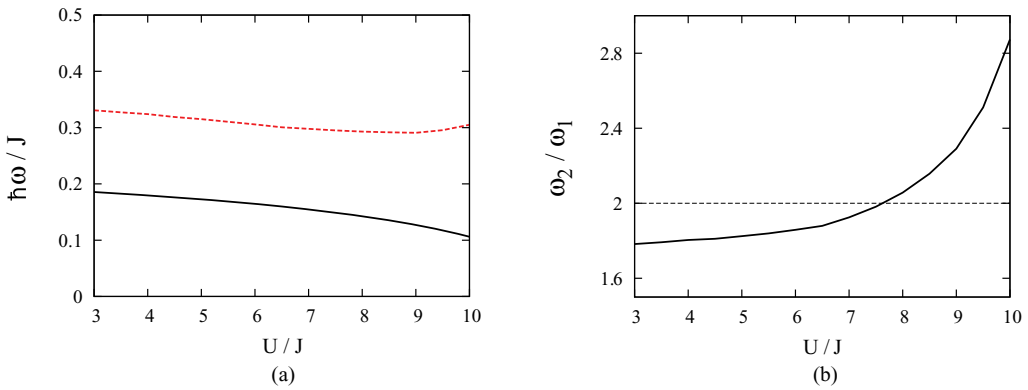

FIG. 8. (Color online) (a) Frequencies of the first mode $\hbar\omega_1/J$ [solid (black) line] and the second mode $\hbar\omega_2/J$ [dashed (red) line] in 1D lattices combined with a parabolic trap. (b) Ratio ω_2/ω_1.

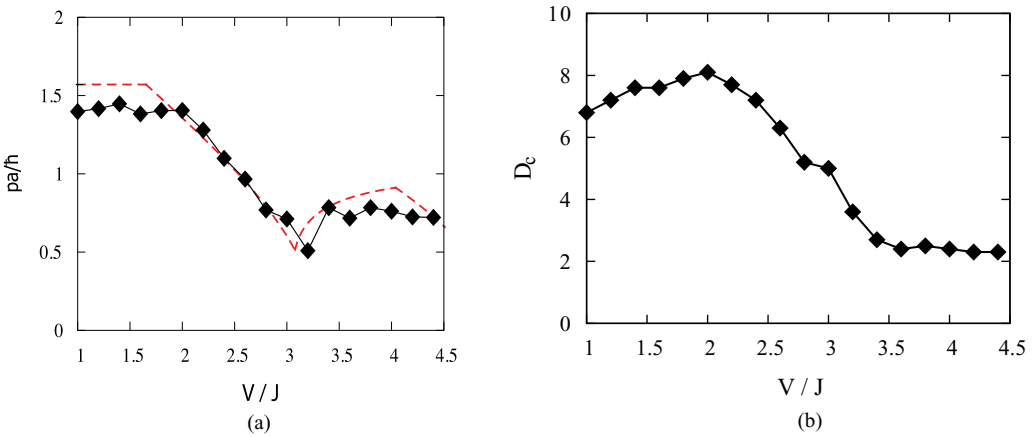

FIG. 10. (Color online) (a) Solid line with symbols represents the maximum local momentum $p_{\max}a/\hbar$ at $D = D_c$ and $t = t_{\max}$ in the system described by Eq. (14) as a function of V/J. The dashed (red) line represents the critical momentum for the DI in the homogeneous case at $\nu = 0.4$ [28]. (b) Critical displacement D_c as a function of V/J.

symbols in Fig. 10(a), we show the maximum local momentum $p_{\max}$ at $D = D_c$ and $t = t_{\max}$ as a function of V. We clearly see that $p_{\max}$ agrees well with the critical momentum for the DI in the homogeneous lattice system at $\nu = 0.4$ obtained in Ref. [28] by applying the same Gutzwiller approximation to the same dipolar hard-core Bose-Hubbard model. $p_{\max}$ takes a distinct minimum at a point close to the transition to the SS state and is significantly smaller in the SS state than in the SF state. We emphasize that the agreement with the homogeneous case is found in the SS state even though there also exists an SF region with a different critical momentum. This can be attributed to the fact that the critical momentum in the SS phase is smaller than that in the SF phase and that the maximum local momentum is always taken at the center of the SS region where the local condensate density is lowest.

Let us discuss the feasibility of identifying the SS state from the critical momentum. If one can measure the local momentum, the above-mentioned properties of the critical momentum in the SS state allow us to distinguish the SS state from other possible states, such as the SF, MI, and density-wave insulating states. However, since it should be easier to measure the critical displacement rather than the critical local momentum, we show the critical displacement as a function of V in Fig. 10(b), where the significant reduction of D_c in the SS state is clearly shown. Thus, we suggest that it is possible to identify the SS state by measuring the critical displacement D_c.

C. Dynamical transition

It was predicted for the homogeneous case in Ref. [28] that when the superflow momentum increases in the SF state near the phase boundary to the SS state, the transition to the SS phase can occur due to the DI caused by excitations with $\mathbf{k} = (\pi,\pi)$. Since the typical experimental setup includes a parabolic trapping potential, it is important to confirm whether or not this dynamical transition induced by superflow occurs in trapped systems. For this purpose, we choose $V = 3.2$ such that the ground state is in the SF state close to the transition point. In Fig. 11(a), we show the density profile of the ground state. Taking this state as the initial state, we compute the dipole-oscillation dynamics of Eq. (14) setting $D = 2$. To

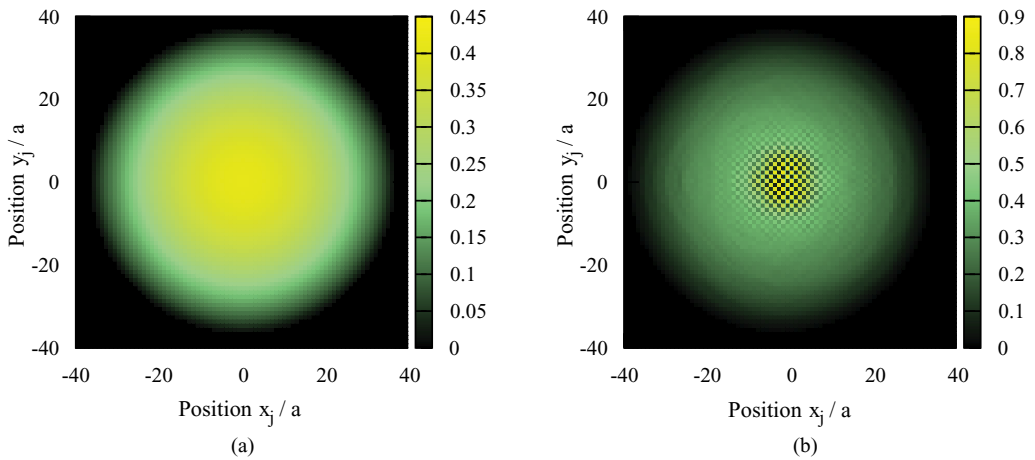

FIG. 11. (Color online) Snapshots of the density distribution n_j during the dipole-oscillation dynamics of Eq. (14) with $V/J = 3.2$, where $Jt/\hbar = 0$ (a) and $Jt/\hbar = 310$ (b).

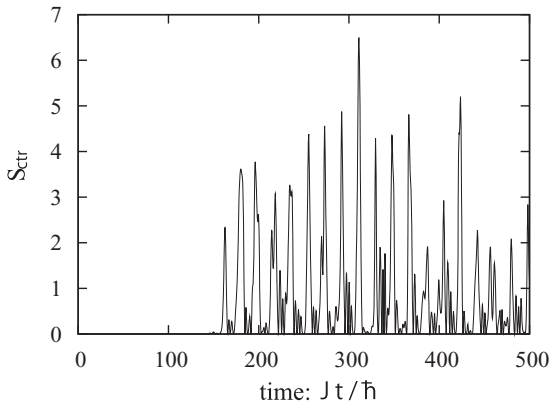

FIG. 12. Time evolution of the structure factor $S_{ctr}(\pi,\pi)$ during the dipole oscillation, where $V/J = 3.2$ and $D = 2$.

quantify the formation of the density-wave order associated with the dynamical transition to the SS, we compute the time evolution of the static structure factor $S_{ctr}(\pi,\pi)$, which is shown in Fig. 12. $S_{ctr}(\pi,\pi)$ exhibits repetitive growth and collapse after the time $t \simeq 150$. In Fig. 11(b), we show the density distribution at $t = 310$, where the growth of the $S_{ctr}(\pi,\pi)$ is most prominent within the time scale plotted in Fig. 12. There we clearly see that the checkerboard density wave forms around the trap center. Thus, the dynamical transition to the SS can occur in the dipole-oscillation dynamics in a trapped system.

VI. SUMMARY

We have studied the SF transport of Bose gases in optical lattices using the Gutzwiller approximation. In 1D, 2D, and 3D homogeneous systems, we determined the critical momenta for the LI and the DI from the excitation spectra. Especially, we have found a DI caused by excitations with short wavelengths in one dimension when the on-site interaction is very small. In a trapped system, we have analyzed the dynamics of dipole oscillations induced by suddenly displacing the trap center. We have found that the critical momentum defined by the maximum local momentum in the trap system quantitatively agrees with that in the homogeneous system at unit filling. We have also shown that a resonance phenomenon is caused by the coupling between the dipole-oscillation mode and the breathing mode. Moreover, we have investigated the critical momentum of dipolar hard-core bosons and shown that the critical momentum of the SS state is smaller than that of the SF state as in the case of the homogeneous system. This result allows us to suggest that the SS state should be identified by measuring the critical displacement. We have, finally, shown that the dynamical transition from the SF state to the SS state can be induced by dipole oscillations.

ACKNOWLEDGMENTS

The authors thank A. Polkovnikov, S. Tsuchiya, and D. Yamamoto for useful comments and discussion.

[1] M. Greiner, O. Mandel, T. Esslinger, T. W. Hänsch, and I. Bloch, Nature **415**, 39 (2002).
[2] I. Bloch, J. Dalibard, and W. Zwerger, Rev. Mod. Phys. **80**, 885 (2008).
[3] T. Stöferle, H. Moritz, C. Schori, M. Köhl, and T. Esslinger, Phys. Rev. Lett. **92**, 130403 (2004).
[4] D. Clément, N. Fabbri, L. Fallani, C. Fort, and M. Inguscio, Phys. Rev. Lett. **102**, 155301 (2009).
[5] P. T. Ernst, S. Götze, J. S. Krauser, K. Pyka, D.-S. Lühmann, D. Pfannkuche, and K. Sengstock, Nat. Phys. **6**, 56 (2009).
[6] U. Bissbort, S. Götze, Y. Li, J. Heinze, J. S. Krauser, M. Weinberg, C. Becker, K. Sengstock, and W. Hofstetter, Phys. Rev. Lett. **106**, 205303 (2011).
[7] X. Zhang, C.-L. Hung, S.-K. Tung, and C. Chin, Science **335**, 1070 (2012).
[8] C. D. Fertig, K. M. O'Hara, J. H. Huckans, S. L. Rolston, W. D. Phillips, and J. V. Porto, Phys. Rev. Lett. **94**, 120403 (2005).
[9] J. Mun, P. Medley, G. K. Campbell, L. G. Marcassa, D. E. Pritchard, and W. Ketterle, Phys. Rev. Lett. **99**, 150604 (2007).
[10] D. McKay, M. White, M. Pasienski, and B. DeMarco, Nature **453**, 76 (2008).
[11] L. Fallani, L. De Sarlo, J. E. Lye, M. Modugno, R. Saers, C. Fort, and M. Inguscio, Phys. Rev. Lett. **93**, 140406 (2004).
[12] L. De Sarlo, L. Fallani, J. E. Lye, M. Modugno, R. Saers, C. Fort, and M. Inguscio, Phys. Rev. A **72**, 013603 (2005).
[13] S. Burger, F. S. Cataliotti, C. Fort, F. Minardi, M. Inguscio, M. L. Chiofalo, and M. P. Tosi, Phys. Rev. Lett. **86**, 4447 (2001).
[14] B. Wu and Q. Niu, Phys. Rev. A **64**, 061603 (2001).
[15] M. Modugno, C. Tozzo, and F. Dalfovo, Phys. Rev. A **70**, 043625 (2004).
[16] E. Altman, A. Polkovnikov, E. Demler, B. I. Halperin, and M. D. Lukin, Phys. Rev. Lett. **95**, 020402 (2005).
[17] A. Polkovnikov, E. Altman, E. Demler, B. Halperin, and M. D. Lukin, Phys. Rev. A **71**, 063613 (2005).
[18] A. Griesmaier, J. Werner, S. Hensler, J. Stuhler, and T. Pfau, Phys. Rev. Lett. **94**, 160401 (2005).
[19] M. Lu, N. Q. Burdick, S. H. Youn, and B. L. Lev, Phys. Rev. Lett. **107**, 190401 (2011).
[20] K.-K. Ni, S. Ospelkaus, M. H. G. de Miranda, A. Pe'er, B. Neyenhuis, J. J. Zirbel, S. Kotochigova, P. S. Julienne, D. S. Jin, and J. Ye, Science **322**, 231 (2008).
[21] K. Aikawa, D. Akamatsu, M. Hayashi, K. Oasa, J. Kobayashi, P. Naidon, T. Kishimoto, M. Ueda, and S. Inouye, Phys. Rev. Lett. **105**, 203001 (2010).
[22] K. Goral, L. Santos, and M. Lewenstein, Phys. Rev. Lett. **88**, 170406 (2002).
[23] D. L. Kovrizhin, C. V. Pai, and S. Sinha, Europhys. Lett. **72**, 162 (2005).
[24] S. Yi, T. Li, and C. P. Sun, Phys. Rev. Lett. **98**, 260405 (2007).
[25] I. Danshita and C. A. R. Sá de Melo, Phys. Rev. Lett. **103**, 225301 (2009).

[26] B. Capogrosso-Sansone, C. Trefzger, M. Lewenstein, P. Zoller, and G. Pupillo, Phys. Rev. Lett. **104**, 125301 (2010).
[27] L. Pollet, J. D. Picon, H. P. Büchler, and M. Troyer, Phys. Rev. Lett. **104**, 125302 (2010).
[28] I. Danshita and D. Yamamoto, Phys. Rev. A **82**, 013645 (2010).
[29] T. Ohgoe, T. Suzuki, and N. Kawashima, J. Phys. Soc. Jpn. **80**, 113001 (2011).
[30] M. P. A. Fisher, P. B. Weichman, G. Grinstein, and D. S. Fisher, Phys. Rev. B **40**, 546 (1989).
[31] D. Jaksch, C. Bruder, J. I. Cirac, C. W. Gardiner, and P. Zoller, Phys. Rev. Lett. **81**, 3108 (1998).
[32] D. S. Rokhsar and B. G. Kotliar, Phys. Rev. B **44**, 10328 (1991).
[33] M. Yamashita and M. W. Jack, Phys. Rev. A **76**, 023606 (2007).
[34] T. D. Kühner, S. R. White, and H. Monien, Phys. Rev. B **61**, 12474 (2000).
[35] K. V. Krutitsky and P. Navez, Phys. Rev. A **84**, 033602 (2011).
[36] C. Trefzger, C. Menotti, and M. Lewenstein, Phys. Rev. A **78**, 043604 (2008).
[37] K. V. Krutitsky, J. Larson, and M. Lewenstein, Phys. Rev. A **82**, 033618 (2010).
[38] D. L. Kovrizhin, G. V. Pai, and S. Sinha, arXiv:0707.2937v1.
[39] B. Wu and Q. Niu, New J. Phys. **5**, 104 (2003).
[40] S. Konabe and T. Nikuni, J. Phys. B **39**, S101 (2006).
[41] K. Iigaya, S. Konabe, I. Danshita, and T. Nikuni, Phys. Rev. A **74**, 053611 (2006).
[42] A. Smerzi, A. Trombettoni, P. G. Kevrekidis, and A. R. Bishop, Phys. Rev. Lett. **89**, 170402 (2002).
[43] It can be proven that if Eqs. (7) and (8) have a solution with a frequency ω and $\mathcal{N} > 0$, they also have a solution with a frequency $-\omega$ and $\mathcal{N} < 0$, which we call the antimode.
[44] A. A. Burkov and A. Paramekanti, Phys. Rev. Lett. **100**, 255301 (2008).
[45] R. Ganesh, A. Paramekanti, and A. A. Burkov, Phys. Rev. A **80**, 043612 (2009).
[46] Y. Yunomae, D. Yamamoto, I. Danshita, N. Yokoshi, and S. Tsuchiya, Phys. Rev. A **80**, 063627 (2009).
[47] M. Snoek and W. Hofstetter, Phys. Rev. A. **76**, 051603(R) (2007).
[48] W. S. Bakr, A. Peng, M. E. Tai, R. Ma, J. Simon, J. I. Cillen, S. Fölling, L. Pollet, and M. Greiner, Science **329**, 547 (2010).